ELSEVIER

Quaternary Science Reviews 25 (2006) 832–845

QSR

The relative role of oceanic heat transport and orography on glacial climate

Vanya Romanova[a,*], Gerrit Lohmann[a,b,c], Klaus Grosfeld[a,c], Martin Butzin[d]

[a]Department of Physics, University of Bremen, 28334 Bremen, Germany
[b]DFG Research Center Ocean Margins (RCOM), University of Bremen, 28334 Bremen, Germany
[c]Alfred Wegener Institute for Polar and Marine Research, 27515 Bremerhaven, Germany
[d]Department of Geosciences, University of Bremen, 28334 Bremen, Germany

Received 20 July 2004; accepted 12 July 2005

Abstract

During the Last Glacial Maximum, the Earth's orography and oceanic heat transport contribute to a cooling in the North Atlantic. By using an atmospheric general circulation model of intermediate complexity, we investigate the sensitivity of the atmospheric temperature and circulation during glacial climate, focussing on the impact of the orography and different oceanic heat transports. The results show a strong dependence of the glacial Northern Hemisphere circulation pattern to the changed orography. The blocking effect of the elevated orography due to the Laurentide Ice Sheet over the North American continent forced a deflection of westerlies, their enhancement and a southward displacement over the Atlantic. Independently, the glacial climate is influenced by the oceanic heat transport. The reduced oceanic heat transport on the glacial climate shows a 20–40% contribution for the total cooling relative to the present-day climate in the North Atlantic and polar regions. Finally, we find that the altered orography in the Northern Hemisphere and different oceanic heat transports result in a changed hydrological cycle, a reduction of the Hadley circulation and a southward shift of the Intertropical Convergence Zone in the boreal winter during glacial times.
© 2005 Elsevier Ltd. All rights reserved.

1. Introduction

The Last Glacial Maximum (LGM) at about 21,000 years B.P. is the period when the most recent glaciation cycle was at its peak. This period is well captured by marine sediment cores, terrestrial climate records and ice-core data (e.g. Jouzel et al., 1987; Farrera et al., 1999; Mix et al., 1999; Alley and Clark, 1999; Bard, 1999; Clark et al., 2002). The abundance of LGM data allows us to reconstruct global sea surface temperature (SST) fields and the sea-ice margins in the Atlantic Ocean. However, various SST reconstructions (e.g. CLIMAP 1981; GLAMAP 2000—German Glacial Atlantic Ocean Mapping Project; Pflaumann et al., 2003; Mix et al., 2001; Sarnthein et al., 2003; Paul and Schäfer-Neth, 2003; Weinelt et al., 1996) differ in the constructing methodology and in the LGM definitions for time intervals, but all suppose climatic stability with maximum glacial sea level low stand.

The CLIMAP (1981) SST and sea-ice reconstruction is characterized by sea-ice margins in Northern Hemisphere reaching far south and a general cooling of the surface waters, except for some areas in the tropical Pacific Ocean, where sea temperatures were higher than present-day values. An additional reduction of CLIMAP SSTs in the tropics (Lohmann and Lorenz, 2000) can provide for consistency with more actual paleo-data (Farrera et al., 1999) and snow lines (Lorenz and Lohmann, 2004). The CLIMAP (1981) reconstruction with applied additional tropical cooling at the surface boundary of an ocean model provokes weakening of the overturning circulation (Prange et al., 2002; Knorr and

*Corresponding author. Tel.: +49 421 218 7186; fax: +49 421 218 7040.
E-mail addresses: vanya@palmod.uni-bremen.de (V. Romanova), gerrit.lohmann@dkrz.de (G. Lohmann), grosfeld@palmod.uni-bremen.de (K. Grosfeld), mbutzin@marum.de (M. Butzin).

0277-3791/$ - see front matter © 2005 Elsevier Ltd. All rights reserved.
doi:10.1016/j.quascirev.2005.07.007

Lohmann, 2003). However, some new reconstructions give evidence for substantially reduced sea ice coverage with vast ice-free areas in the Nordic Seas (Weinelt et al., 1996; de Vernal and Hillaire-Marcel, 2000; Sarnthein et al., 2003; Paul and Schäfer-Neth, 2003). The GLAMAP 2000 (Pflaumann et al., 2003; Sarnthein et al., 2003; Paul and Schäfer-Neth, 2003) and Weinelt et al. (1996) SST reconstructions, taken as boundary conditions to an ocean general circulation model (OGCM), provoke even more intense overturning strength compared to the present-day simulation (Romanova et al., 2004; Prange et al., 2004), which maintains the warm temperatures in the Nordic Seas. To examine the atmospheric response to different oceanic background conditions, we use the corresponding heat transports, as obtained from an OGCM integrated under LGM conditions, to force an atmospheric general circulation model (AGCM).

During the LGM the orography over North American and European continents was altered due to the highly elevated Laurentide, Fennoscandian and Barents Sea Ice Sheets. Along with the modified thermal forcing, the changed orography over North America can strongly influence the atmospheric circulation causing splitting of the zonal flow and its deviation from the present-day circulation (Kutzbach and Wright, 1985; Manabe and Broccoli, 1985; Broccoli, 2000). As well, the blocked entrance of the Barents Sea and the build-up of continental ice on the Barents Sea shelf during LGM can influence the hydrological cycle over northwest Europe and have a significant impact over North Atlantic Ocean (Pflaumann et al., 2003).

The relative importance of thermal and orographic forcing upon dependence of the strength of zonal mean flow upon the extratropical stationary wave field has been investigated by several authors. Using an AGCM, Nigam et al. (1987) found that the orographical factor has two times greater influence than the heating factor in the upper troposphere, and that their contributions are equal for the lower troposphere. Other authors (Valdes and Hoskins, 1989; Chen, 2000) found predominance of the thermal factor for maintaining the extratropical stationary wave structure in the lower troposphere. Held and Ting (1990) pointed out that the dominance of each factor depends mainly on the strength of the low-level mid-latitude westerlies. Using a coupled atmosphere-ocean climate model, Kim (2004) investigated the effect of the ice sheet topography and the change of CO_2 concentration on the LGM climate. He found that climate cooling of the LGM is more than half that due to the reduction of the atmospheric CO_2.

This study, therefore, provides LGM simulations forced with oceanic heat transports, based on different glacial reconstructions, and concentrates on the sensitivity of the atmospheric circulation system to: (i) different thermal forcing conditions; (ii) large-scale orographic obstacles such as the Laurentide Ice Sheet over North American continent; and (iii) the glacial atmospheric CO_2 reduction. Its objective aim is to deconstruct the effects of orographically and thermally induced responses and to assess the significance of each factor for the modified flow regime compared to the present-day conditions. The paper is organized as follows: the second section gives a description of the methodology and the experimental set-up, and the third section shows the results. The results are discussed in Section 4, and the conclusions are given in Section 5.

2. Methodology

2.1. Boundary conditions

The present-day simulation is forced with SST and ice compactness taken from the Atmospheric Model Intercomparison Project (AMIP) (Phillips et al., 1995). The temperature fields represent climatological averages for the time period from 1979 to 1994. The CLIMAP (1981) SST and sea-ice extent reconstruction for the LGM, based on foraminiferal assemblages, is taken as a boundary condition for simulating glacial conditions. The validity of CLIMAP reconstruction is strongly discussed, especially in the tropical areas (e.g. Farrera et al., 1999; Mix et al., 1999; Bard, 1999) indicating too warm SSTs. Hence, one experiment is carried out forced with CLIMAP (1981) SSTs but additional cooling of 3 °C in the tropics. This experiment aims to reduce the temperature discrepancies between marine and terrestrial proxy data for the LGM. The new reconstruction, GLAMAP 2000, provides SSTs and sea-ice margins for another boundary condition. In this reconstruction, the winter sea ice extent is similar to the CLIMAP summer sea ice margin and the Nordic Seas are ice-free during summer months. The average surface temperature in the Atlantic Ocean is by 0.7 °C higher than in the CLIMAP reconstruction.

The glacial runs use glacial orography, land-sea and glacier masks (Peltier, 1994). The CO_2 concentration is fixed to 360 ppm for the present-day experiment and is reduced to 200 ppm for the glacial run according to observational values (e.g. Barnola et al., 1987; Keeling et al., 1996). The Earth's obliquity, orbital eccentricity and vernal equinox mean longitude of perihelion for the present day and glacial runs are taken for the years 2,000 year A.D. and 21,000 year B.P., respectively, and are calculated according to Berger (1978).

2.2. Ocean circulation model

The above mentioned SSTs and sea-ice cover are applied to the AGCM ECHAM3/T42 (Roeckner et al., 1992; Lohmann and Lorenz, 2000). The resulting monthly averaged surface air temperatures, surface

freshwater fluxes and wind stresses serve as forcing fields for the OGCM Large Scale Geostrophic (LSG), (Maier-Reimer et al., 1993). The ocean model integrates the momentum equations, including all terms except the nonlinear advection of momentum. It has a horizontal resolution of $3.5^\circ \times 3.5^\circ$ and 11 vertical levels. The advection scheme for the temperature and salinity is a third-order QUICK scheme (Leonard, 1979; Schäfer-Neth and Paul, 2001; Prange et al., 2003). Vertical diffusivity is explicitly prescribed ranging from $0.3\,\mathrm{cm^{-2}\,s^{-1}}$ at the surface up to $3.2\,\mathrm{cm^{-2}\,s^{-1}}$ in the abyssal ocean, as obtained from simulations of oceanic radiocarbon (Butzin et al., 2003). A heat flux parameterization is applied, which allows for scale selective damping of surface temperature anomalies (Prange et al., 2003) and the free evolution of the SSS (sea surface salinity). The model includes a parameterization of overflow. The glacial sea level is reduced by 120 m, the Bering Strait is closed and the Barents Sea is ice covered, leading to a blocking of the ocean currents in these regions. The equilibrium states are obtained after 5500 years of model integration, initialized with present-day conditions and with an additional global salinity increase of 1 psu. The 10 years monthly averaged SST fields, as simulated by the ocean model, are applied to the bottom boundary of the AGCM PUMA.

2.3. Atmospheric circulation model

The atmospheric model used in the present study is Portable University Model of Atmosphere (PUMA) developed at the University of Hamburg (Fraedrich et al., 1998; Lunkeit et al., 1998). The dynamical core of PUMA is based on the multi-layer spectral model proposed by Hoskins and Simmons (1975). It integrates the primitive equations formulated in terms of the vertical component of the absolute vorticity, the horizontal divergence, the temperature, the logarithm of the surface pressure and the specific humidity. The equations are solved using the spectral transform method (Orszag, 1970; Eliasen et al., 1970). The calculations are evaluated on a longitude/latitude T21 grid of 64 by 32 points, which corresponds approximately to 5.6° in Gaussian coordinates. Five equally spaced, terrain-following sigma levels are used in the vertical direction. The surface fluxes of moisture, heat and momentum are calculated with bulk formulas. Parameterizations for the land and soil temperatures, soil hydrology and river runoff are implemented in the model.

PUMA is classified as a model of intermediate complexity (Claussen et al., 2002) and it is designed to be comparable with comprehensive AGCMs like ECHAM (Roeckner et al., 1992). Previously, it was used for evaluation of stormtracks and baroclinic life cycles (e.g. Frisius et al., 1998; Franzke et al., 2000) for investigating the atmospheric response during deglaciation (Knorr et al., 2005), and it is shown that the results are comparable to other AGCM simulations (Grosfeld et al., 2005, pers. comm.).

The AGCM is coupled to a mixed layer (slab) ocean model. The mixed-layer temperature T_{mix} is calculated following the equation:

$$\frac{\mathrm{d}T_{\mathrm{mix}}}{\mathrm{d}t} = \frac{Q_{\mathrm{atm}} + Q_{\mathrm{ocean}}}{\rho_w c_{\rho_w} h_{\mathrm{mix}}}, \tag{1}$$

where ρ_{w} and $c_{\rho_{\mathrm{w}}}$ are the water density and the heat capacity, respectively. The mixed layer depth h_{mix} is fixed at 50 m. The atmospheric heat flux Q_{atm} is the sum of the net short-wave and long-wave radiative energy fluxes, the sensible heat flux and the latent heat flux due to evaporation. The oceanic heat flux Q_{ocean} is monthly prescribed in the experimental set-up. The coupled system, forced with prescribed oceanic heat transport, allows prediction of the sea surface temperature. A simple thermodynamic sea ice model is implemented into the system.

2.4. Experimental set-up

To simulate the atmospheric present-day and glacial conditions, we perform numerical experiments using at first the PUMA with prescribed SSTs and sea-ice extend. The equilibrium states are obtained after 50 years integration. The present-day experiment using initially the AMIP forcing is denoted with ***AMIP***, and the glacial simulations are indicated with: ***CLIMAP*** for the simulation with CLIMAP forcing; ***CLIMAPc*** for the simulation with CLIMAP and additional tropical cooling; and ***GLAMAP*** for the experiment with GLAMAP 2000 boundary conditions (Table 1).

To calculate the surface heat fluxes Q_{atm}, monthly averages over the last ten modeled years from the experiments with prescribed surface boundary conditions are estimated. These fluxes are applied to the mixed layer ocean model. The heat flux from ***AMIP*** is used for five coupled experiments (Table 1): a present-day experiment (hereafter called the ***control*** run); two glacial experiments with orography given by Peltier (1994), the first one with CO_2 equal to 200 ppm (***Lau_200***) and the second CO_2 equal to 360 ppm (***Lau_360***); and two experiments with implemented half height of the Laurentide Ice Sheet with 200 ppm (***halfLau_200***) and 360 ppm (***halfLau_360***) CO_2. To visualize the different orography used to force the sensitivity experiments as represented in the model grid, the surface geopotentials for the present-day, the half of the height and the full height of the Laurentide Ice Sheet are shown in Fig. 1. The difference of the corresponding atmospheric patterns gives the isolated effect of the changed orographic forcing and the effect of changed atmospheric carbon dioxide concentration. The next

Table 1
Overview of numerical experiments and their set-up

Prescribed surface temperatures	Set-up	CO_2 (ppm)	Orbital parameters	Orography	Abbreviation
AMIP	PD	360	2000 y A.D.	Present-day	***AMIP***
CLIMAP	LGM	200	21,000 y B.P.	Peltier (1994)	***CLIMAP***
CLIMAP with tropical cooling	LGM	200	21,000 y B.P.	Peltier (1994)	***CLIMAPc***
GLAMAP 2000	LGM	200	21,000 y B.P.	Peltier (1994)	***GLAMAP***
AGCM + ML experiments with prescribed heat fluxes					
10 years averaged surface heat fluxes from exp. ***AMIP***	PD	360		Present-day	***control***
	LGM	200	21,000 y B.P.	Peltier (1994)	***Lau_200***
	Sensitivity exp.	360	21,000 y B.P.	Peltier (1994)	***Lau_360***
	LGM	200	21,000 y B.P.	1/2 Laurentide Ice Sheet	***halfLau_200***
	Sensitivity exp.	360	21,000 y B.P.	1/2 Laurentide Ice Sheet	***halfLau_360***
10 years averaged surface heat fluxes from exp. ***CLIMAP***	LGM	200	21,000 y B.P.	Peltier (1994)	***LGM_CL***
10 years averaged surface heat fluxes from exp. ***CLIMAPc***	LGM	200	21,000 y B.P.	Peltier (1994)	***LGM_CLc***
10 years averaged surface heat fluxes from exp. ***GLAMAP***	LGM	200	21,000 y B.P.	Peltier (1994)	***LGM_GL***

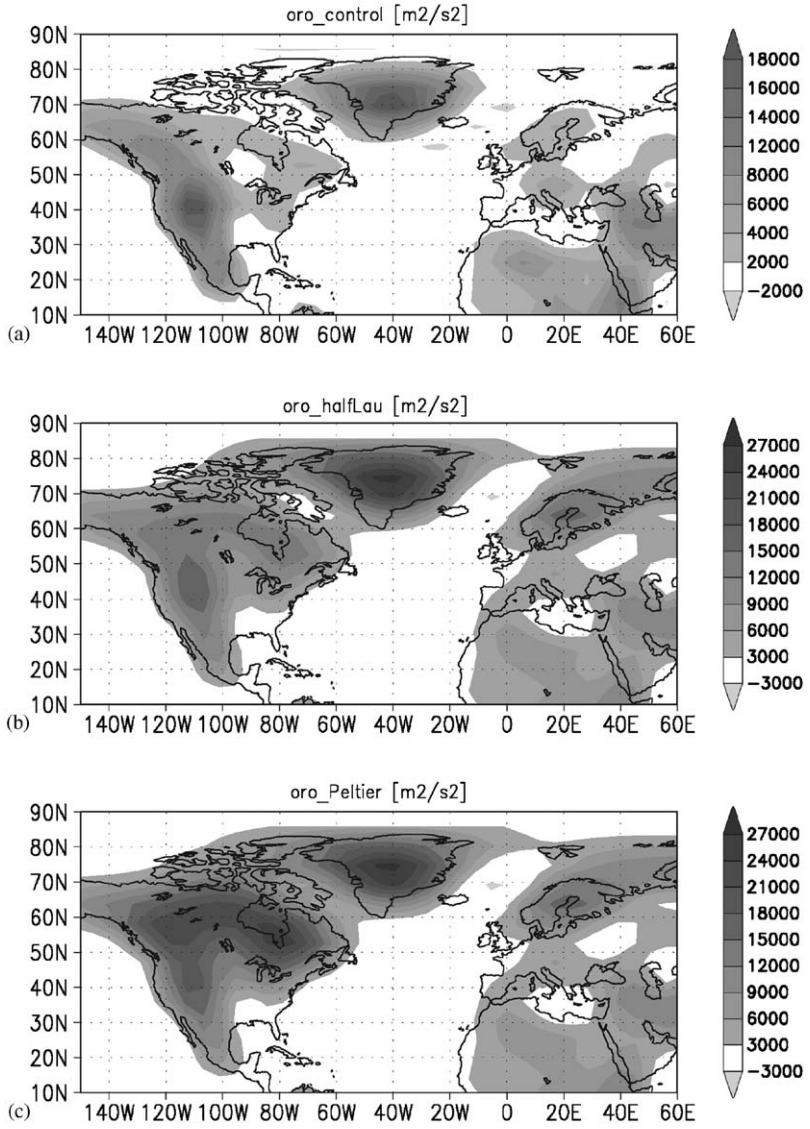

Fig. 1. Surface geopotential ($m^2 s^{-2}$) for: (a) the ***control*** run; (b) the exp. with half of the height of the Laurentide Ice Sheet; (c) the exp. with full height of the Laurentide Ice Sheet.

three experiments (***LGM_CL***, ***LGM_CLc*** and ***LGM_GL***) represent the glacial set-up, using heat fluxes taken from the glacial experiments with prescribed sea surface temperatures ***CLIMAP***, ***CLIMAPc*** and ***GLAMAP***, respectively. The latter climatological means, obtained through different thermal forcing, extract the effect of the different oceanic heating on the atmospheric circulation systems.

3. Results

3.1. The North Atlantic meridional overturning and the oceanic heat transport

The overturning circulations in the Atlantic Ocean as simulated with the OGCM LSG for the present-day simulation and the glacial experiments are shown in Fig. 2. The maximum transport of the overturning cell is strongest for the present-day ocean and equal to 20 Sv ($1\ \mathrm{Sv} = 1 \times 10^6\ \mathrm{m^3\ s^{-1}}$). The meridional overturning for the glacial experiments depends on the glacial reconstruction used as a boundary condition. The experiments forced with CLIMAP and GLAMAP 2000 reconstructions yield maximum overturning rates of about 18 Sv. These experiments differ in the location of the NADW (North Atlantic Deep Water) formation (Fig. 2b and d). The Nordic Seas are ice-free for the summer months in the GLAMAP 2000 reconstruction, which allows NADW to be formed further to the north (Fig. 2d). The experiment forced with the coldest boundary conditions—CLIMAP with additionally applied cooling in the tropics—gives 50% (around 10 Sv) reduction of the North Atlantic maximum overturning strength compared to the present-day simulation (Fig. 2c).

Along with the overturning rates, the meridional heat transports in the Atlantic basin differ in the four experiments. At 30°N, the oceanic heat transport is 0.5 PW ($1\ \mathrm{PW} = 10^{15}$ W) for the experiment performed with the coldest SST (CLIMAPc). The experiment forced with the original CLIMAP reconstruction (Fig. 2b) has a meridional heat transport of 0.8 PW. The highest value is represented by the glacial experiment forced with GLAMAP 2000 at 0.9 PW. All glacial runs possess reduced heat transports compared to the

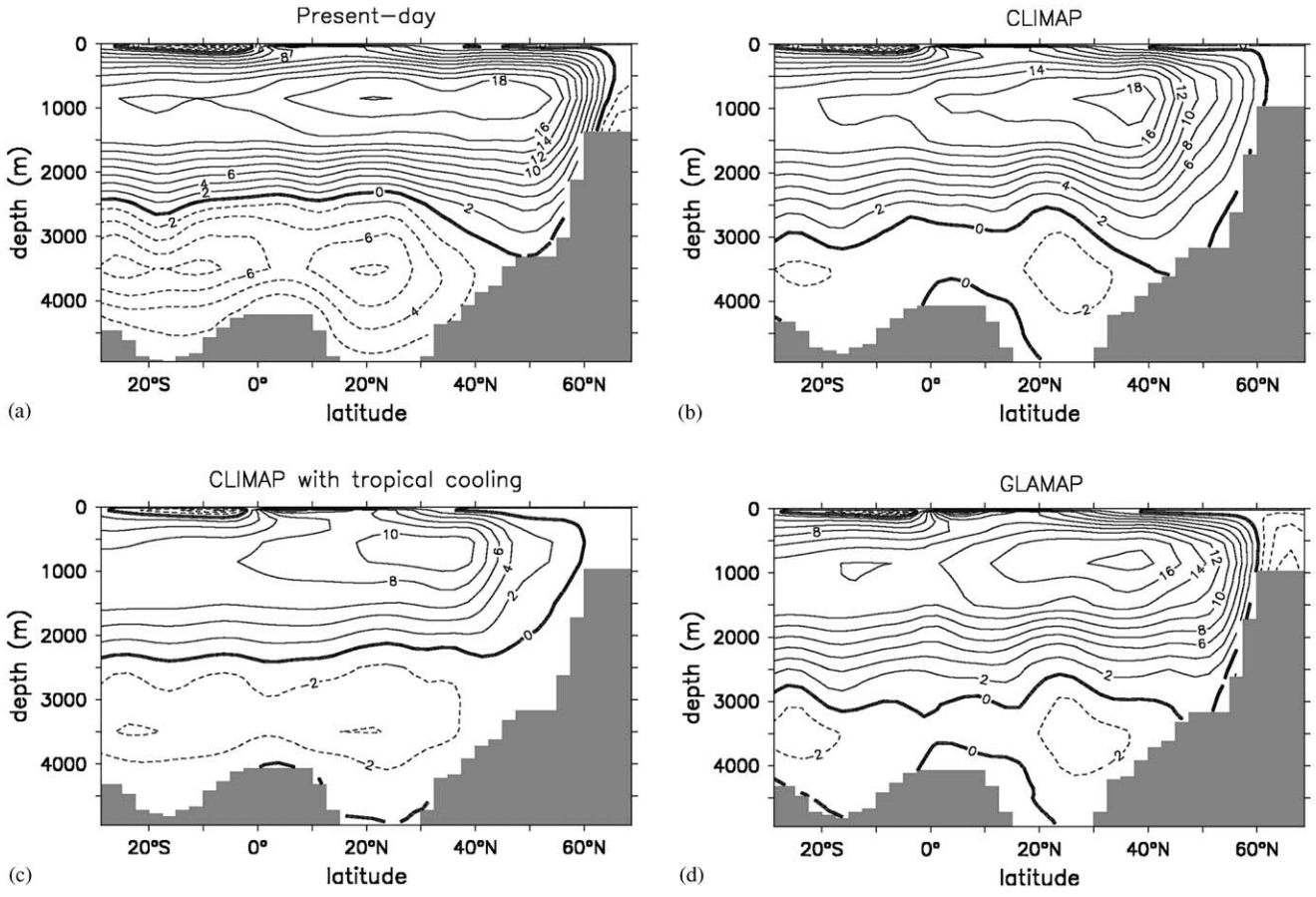

Fig. 2. Atlantic meridional overturning stream function for experiments (a) present-day simulation; (b) LGM exp. forced with the CLIMAP reconstruction (***LGM_CL***); (c) LGM exp. forced with the CLIMAP reconstruction with additionally applied tropical cooling (***LGM_CLc***); and (d) LGM exp. forced with the GLAMAP 2000 reconstruction (***LGM_GL***). Units are in Sv ($1\ \mathrm{Sv} = 1 \times 10^6\ \mathrm{m^3\ s^{-1}}$).

present-day simulation (1.0 PW). The divergences of these oceanic heat transports, represented as Q_{ocean}, are taken as basis of the atmospheric simulations.

3.2. Surface air temperatures (SAT)

3.2.1. Mixed layer experiments versus prescribed SST experiments

Global mean surface air temperatures for the simulations with prescribed SSTs and for the experiments performed with a coupled mixed-layer ocean are shown in Fig. 3. Lowering of global temperatures (of around 1 °C) is found for the model runs performed with the coupled model, compared to the experiments forced with prescribed SSTs. The spatial surface temperature patterns and the surface heat fluxes for the experiments with prescribed SST are very similar to the respective ones performed with the mixed layer ocean (not shown). Since the discrepancies in the SSTs are small, we presume that the slab ocean representation yields an adequate heat balance to assure a stable climatological forcing. In the further discussion, we therefore consider only the experiments performed with PUMA coupled to a mixed layer ocean. The global surface temperature lowering as a result of the reduction of CO_2 from the present-day value of 360 ppm to 200 ppm is around 0.5 °C (Fig. 3, cf. exp.: 1) ***Lau_360*** and ***Lau_200***; and 2) ***halfLau_360*** and ***halfLau_200***). A similar reduction (0.3 °C) of the global surface temperature is provoked by the change of the orography from half of the height of the Laurentide Ice Sheet to full height of the Laurentide Ice Sheet (Fig. 3, cf. exp.: 1) ***halfLau_360*** and ***Lau_360***; and 2) ***halfLau_200*** and ***Lau_200***).

Comparing the SAT of the glacial experiments (***Lau_200***, ***LGM_CL***, ***LGM_CLc*** and ***LGM_GL***) to the present-day experiment, a global temperature lowering is found (Fig. 3), which is a consequence of the combined effect of the glacial experimental set-up, orbital parameters, glacial ice sheets, and reduced CO_2. The difference between the glacial experiments in the SAT values is solely due to the difference in the oceanic heating. The highest value of the global SAT is found for experiment ***Lau_200***, forced with a present-day heat transport but glacial set-up, and the lowest value for experiment ***LGM_CLc***, forced with the heat transport resulting from the experiment with CLIMAP with additional cooling in the tropics (***CLIMAPc***).

3.2.2. Comparison of the modeled present-day climate to data

To validate the present-day simulation we use an extend SST data set after Kaplan et al. (1981). The data set represents 145 years of analyzed global SST anomalies (with regards to normals of 1951–1980) on a $5^\circ \times 5^\circ$ grid. The monthly SST anomalies were added to the AMIP climatology (Phillips et al., 1995) and the averaged DJF temperatures are plotted in Fig. 4b. As the SST spatial pattern of the control run (Fig. 4a) is similar to the SST pattern over the observational period, our heat flux forced climate simulation can be taken as an adequate representation of the present-day climate. The averaged SST differences between the model and the observational data are 0.64 °C, 0.07 °C and 0.58 °C for the Atlantic, Pacific and Indian oceans, respectively.

3.2.3. Spatial temperature differences

The spatial pattern of the SAT differences between experiments ***Lau_200***, ***halfLau_200***, ***Lau_360*** and ***halfLau_360*** and the ***control*** run are shown in Fig. 5. Strong cooling of −16 °C is found over North American

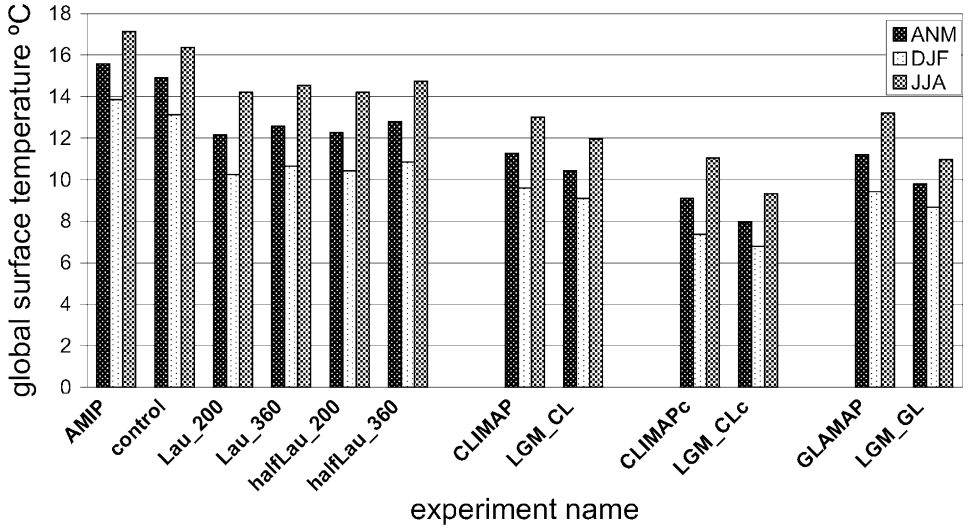

Fig. 3. Annual mean, summer and winter global surface air temperatures averaged over a period of 25 years of integration for the different experiments (***AMIP***, ***CLIMAP*** and ***GLAMAP*** forced with prescribed SST, and ***control***, ***Lau_200***, ***Lau_360***, ***halfLau_200***, ***halfLau_360***, ***LGM_CL***, ***LGM_CLc*** and ***LGM_GL*** performed with PUMA coupled to a slab ocean, Table 1).

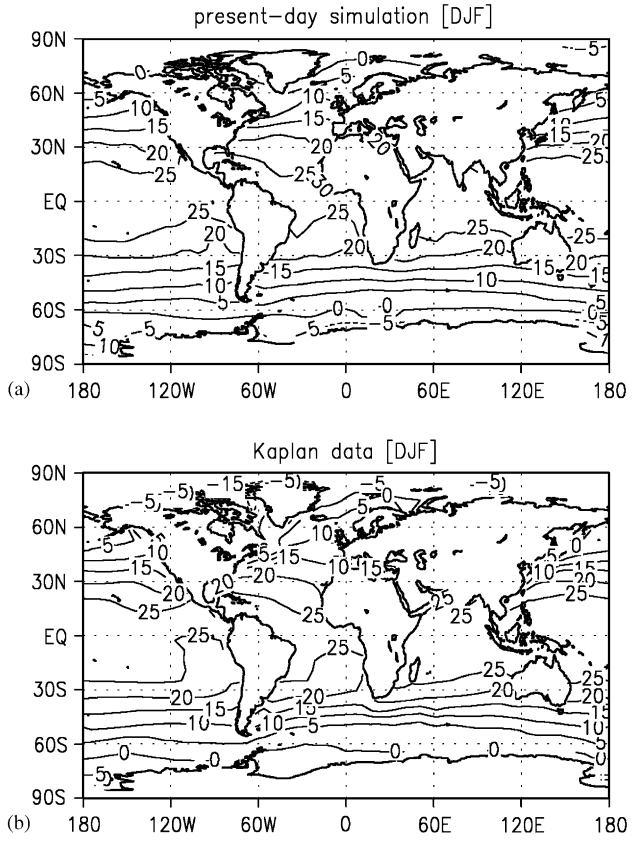

Fig. 4. Sea surface temperature (a) ***control*** run (averaged over a period of 25 years); (b) Kaplan et al. (1998) data set.

continent, which is provoked only from the half of the height of the Laurentide Ice Sheet and the ice albedo (Fig. 5c). Simulating a climate with the full height of the Laurentide Ice Sheet adds another −4 °C to the North American cooling (Fig. 5a), thus the temperature is reduced to −20 °C. The estimates of the SAT anomalies relative to the present-day climate in different latitudinal belts (Table 2) show the effect of CO_2 reduction which is comparable to the effect of the elevation increase of the Laurentide Ice Sheet to its maximum height.

All glacial simulations exhibit strong continental cooling in the mid-latitudes in the Northern Hemisphere (for all simulations the values are about: Europe −10 °C, Siberia −15 °C, North America −20 °C and Greenland −30 °C; not shown). The differences between the experiments appear mainly in the tropics. The coldest experiment ***LGM_CLc*** exhibits a decrease of the tropical zonal mean SAT of around −6 °C compared to the ***control*** run, whereas the experiments ***LGM_CL*** and ***LGM_GL*** show a decreases of 3 °C only (Table 2). The spatial SAT anomalies relative to the glacial experiment forced with present-day oceanic heat transport (Fig. 6a,c) show positive anomalies of around 1 °C in the tropical regions for the experiments ***LGM_CL*** and ***LGM_GL***.

3.3. Consequences of different SST forcings on the atmospheric circulation

The global sea level pressure (SLP) pattern over the Northern Hemisphere is relatively well captured in the present-day experiment (***control*** run) (Fig. 7a). The model simulates the bipolar pressure structure in the North Atlantic, however, its strength is slightly underestimated in the present-day experiment. Its deepening appears not as strong as the observational data, due to the coarse model resolution. The Azores High, the Aleutian Low and the Siberian High are well captured by the model, giving a reasonable climatology (Fig. 7a). The glacial SLP distributions in experiments ***Lau_200*** (Fig. 7b), ***LGM_CLc*** (Fig. 7d), ***LGM_CL***, and ***LGM_GL*** (both not shown) differ from the present day pattern due to the higher glacier elevation, affecting especially the orography over North America. A high-pressure center is situated over the North American continent, which is in contrast to present-day conditions. The Icelandic Low is deepened and shifted to the south-eastern part of the North Atlantic. Thus, the meridional pressure gradient structure is strengthened and dislocated from the present-day configuration. A strong ridge in the sea level isobars is located along the eastern coast of North America, indicating strong advection of warm air from the tropics. The high pressure center over the elevated orography of the North American continent is located oppositely to the Siberian High, and the Aleutian Low is situated against the Icelandic Low pressure. The regular alternation of the highs and lows under glacial conditions provide a wavelike structure of the pressure formations, a feature which is lacking in the present-day climatology. In Fig. 7c, the sea level pressure field is shown for experiment ***halfLau_200***, experiencing only half of the height of Laurentide Ice Sheet. The zonal pressure structure in this case is already disturbed and the anomalous high isobaric center over the North American continent is already formed.

The annual mean present-day and glacial surface wind patterns in the Northern Hemisphere are shown in Figs. 8a,b. Enhanced westerlies over the Atlantic Ocean caused by the enhanced strength of the pressure gradient between Icelandic Low and Azores High are representative for the simulated glacial set-ups (Fig. 8b for experiment ***Lau_200***) compared to the ***control*** run (Fig. 8a). The atmospheric flow, originating from the Pacific Ocean, turns to the north and is tending to overpass the glacier's orography along with the barotropic vorticity balance. After entering the American continent, the flow sets southward in anticyclonic rotation. Over central North America it turns to a cyclonic circulation and enters the Atlantic Ocean, where it is strengthened by the enhanced pressure gradient. The axes of the westerlies over the Atlantic are oriented in south-

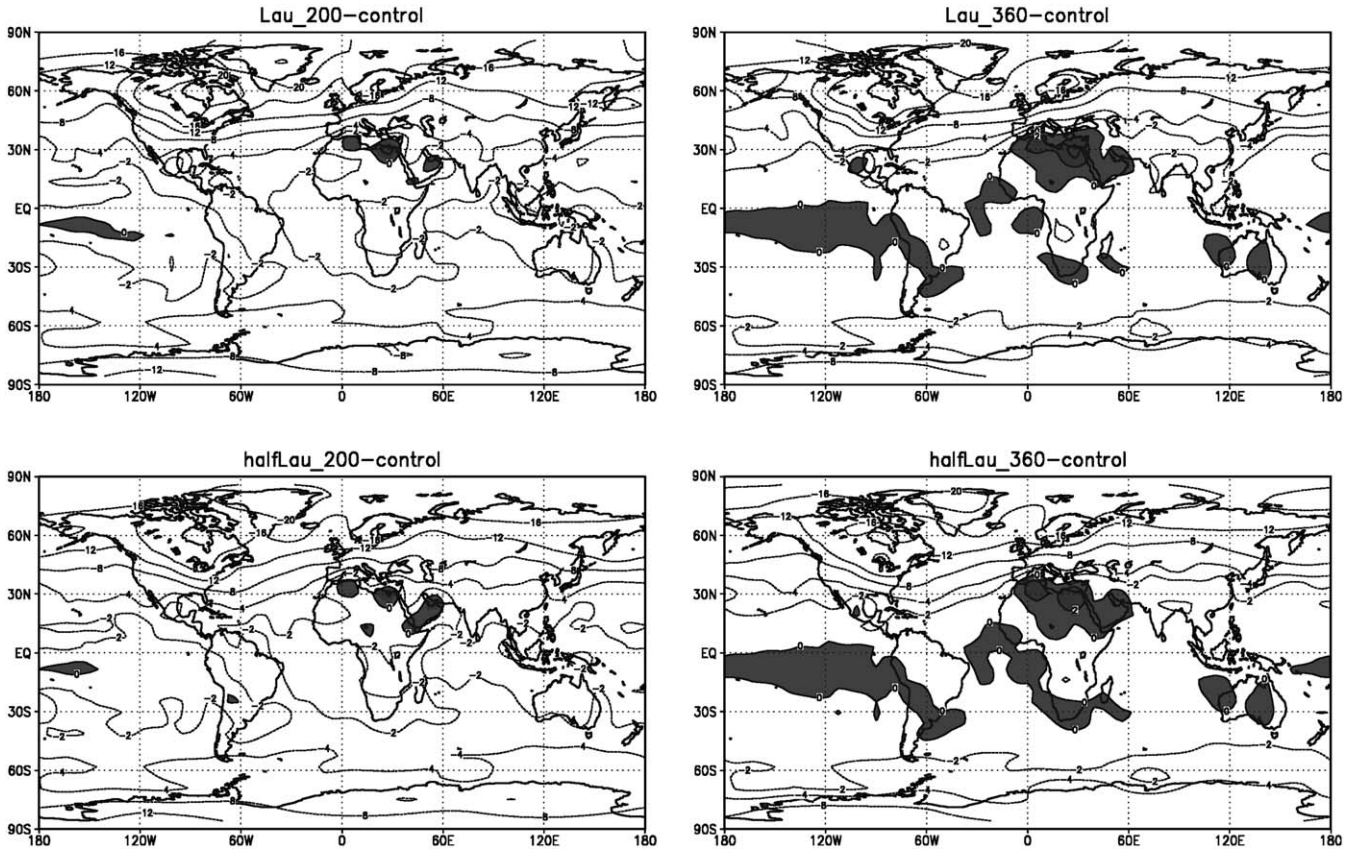

Fig. 5. Spatial pattern of the annual mean surface air temperatures anomalies between the experiments: (a) ***Lau_200–control***; (b) ***Lau_360–control***; (c) ***halfLau_200–control***; (d) ***halfLau_360–control***. (Contour intervals: 1 °C for SAT > 0 °C; 2 °C for 0 °C > SAT > −4 °C; and 4 °C for −4 °C > SAT.)

Table 2
Annual mean surface air temperatures (SAT) anomalies with respect to the ***control*** run calculated over different global latitudinal belts and over the Atlantic and Pacific Oceans

		Tropics 30°S–30°N (°C)	Mid-latitudes 30°N–60°N (°C)	Polar regions 60°N–90°N (°C)
Global	***Lau_200*–control**	−2.14	−9.20	−18.98
	***Lau_360*–control**	−0.79	−6.89	−16.93
	***HalfLau_200*–control**	−1.80	−9.08	−17.54
	***HalfLau_360*–control**	−0.52	−6.63	−15.33
	LGM_CL−control	−3.46	−13.55	−24.62
	LGM_CLc−control	−6.20	−15.14	−26.01
	LGM_GL−control	−2.69	−11.80	−22.96
Atlantic	***Lau_200*–control**	−2.17	−8.78	−19.33
	***Lau_360*–control**	−0.84	−6.89	−17.37
	***HalfLau_200*–control**	−2.06	−8.45	−17.57
	***HalfLau_360*–control**	−0.80	−6.59	−16.13
	LGM_CL−control	−3.59	−13.29	−24.85
	LGM_CLc−control	−6.18	−14.55	−26.57
	LGM_GL−control	−3.32	−11.17	−23.14
Pacific	***Lau_200*–control**	−2.00	−7.69	−11.59
	***Lau_360*–control**	−0.76	−5.11	−9.35
	***HalfLau_200*–control**	−1.90	−6.90	−10.94
	***HalfLau_360*–control**	−0.74	−4.80	−8.50
	LGM_CL−control	−3.06	−14.04	−18.99
	LGM_CLc−control	−5.52	−14.65	−19.66
	LGM_GL−control	−2.08	−11.74	−17.18

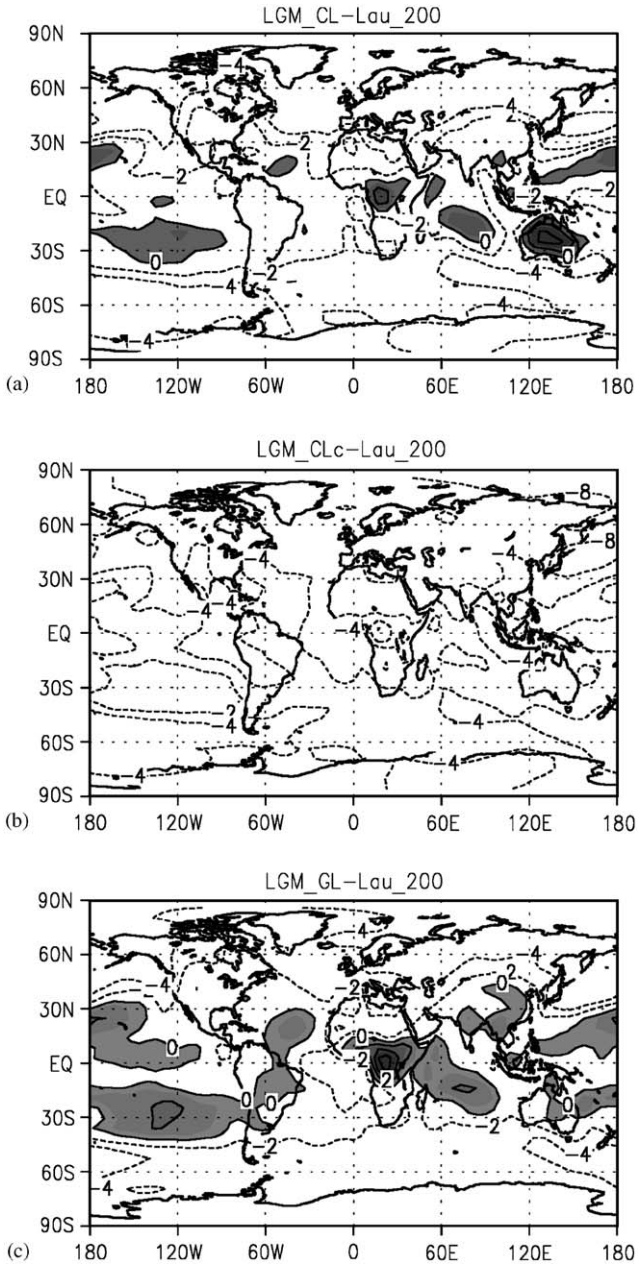

Fig. 6. Spatial pattern of annual mean surface air temperatures anomalies between LGM exp. forced with three different oceanic heat flux patterns and the LGM exp. forced with present-day heat fluxes: (a) ***LGM_CL–Lau_200***; (b) ***LGM_CLc–Lau_200***; (c) ***LGM_GL–Lau_200***. (Contour intervals: 1 °C for SAT > 0 °C; 2 °C for 0 °C > SAT > −4 °C; and 4 °C for −4 °C > SAT).

west–northeast direction and shifted to the south. In the control run, the axes of the westerlies stay clearly zonal and are located more to the north.

The surface circulation over North America depends on the height of the Laurentide Ice Sheet (Fig. 8c, exp. ***halfLau_200***). The westerlies also divert their trajectories due to the blocking effect of the orography in experiment ***halfLau_200***, but not as pronounced as in the glacial experiments. Their strengthening in the North Atlantic is in between the present-day and the glacial one.

3.4. The zonal mean precipitation

To assess different representations of the Hadley circulation and the Intertropical Convergence Zone (ITCZ) for the different glacial reconstructions, the zonal mean precipitation is calculated. The boreal summer and winter zonal mean precipitation values as a function of the latitude are shown in Fig. 9a,b. The region of maximum precipitation in the boreal summer for the present-day simulation is situated in the Northern Hemisphere, while in boreal winter it is located in the Southern Hemisphere. All the year round it stays close to the equator. The modeled JJA precipitation is in a good agreement with the summer climatological estimates of Jaeger (1976) (Fig. 9b). The winter precipitation profiles of the ***control*** run are consistent over the Northern Hemisphere and equatorial region (Fig. 9a), but differ substantially over the Southern Ocean. The precipitation maximum at 60°S could be due to uncertainties in the measured data and/or it cannot be reproduced by the model due to its coarse resolution. Under glacial conditions, more pronounced seasonality is detected. In the boreal summer the precipitation maximum has shifted deeper to the north and in boreal winter deeper to the south. In the temperate latitudes of the Northern Hemisphere the influence of the Laurentide Ice Sheet is seen, leading to a distinct decrease in glacial precipitation.

4. Discussion

The different glacial reconstructions provide different steady states of the ocean circulation with a definite overturning strength. The forcing 'CLIMAP with tropical cooling' produces a weak Atlantic overturning circulation relative to that under present-day conditions. The lowered tropical energy release to the atmosphere, resulting from the imposed tropical cooling in this experiment (***LGM_CLc***), reduces the capability of the atmosphere to export heat to the north. Thus, the atmospheric circulation leads to a uniform cooling of the globe in experiment ***LGM_CLc*** (about 7 °C compared to ***control*** run, Fig. 2), and the weak oceanic heat transport in the North Atlantic allows the occurrence of ice formation far to the south. The glacial simulations ***LGM_CL*** and ***LGM_GL***, using the oceanic heat transport generated by the ocean experiments with a stronger overturning circulation, are associated with ice-free conditions in the Nordic Seas during summer. The increase of the SAT mainly in the tropical Pacific Ocean is an effect of the high tropical temperatures in the CLIMAP and GLAMAP 2000 reconstruc-

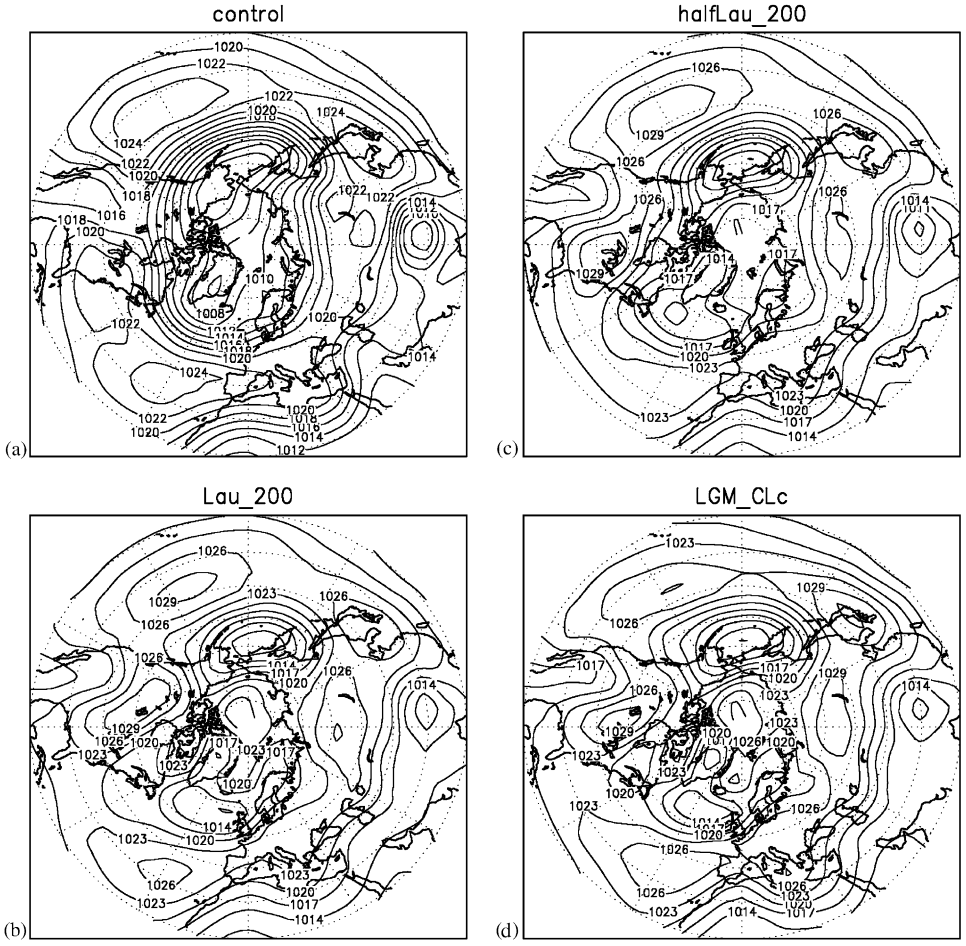

Fig. 7. Annual mean sea level pressure for (a) the ***control*** run; (b) ***Lau_200***; (c) ***halfLau_200*** and (d) ***LGM_CLc*** experiments. Units are hPa. The fields are averaged over 25 years of integration.

tions. The latter is implicitly connected with the enhanced evaporative conditions and water vapour export from the Atlantic Ocean (Lohmann and Lorenz, 2000). The composed effect of changed land ice sheets, oceanic heat transport and hydrology during glacial times affect the tropics by displacing the ITCZ to the south, as shown by coupled and uncoupled model studies (Lohmann, 2003; Chiang et al., 2003). Reduced zonal mean precipitation in all glacial simulations prompt for a weaker Hadley circulation and deeper shifts of the ITCZ towards both sides of the equator (Fig. 9).

The altered orography during the LGM induces completely different glacial SLP patterns compared to present-day. A new high-pressure center is located over northern North America, which is related to the elevations of the glaciers and appears to be a robust feature for the LGM climate. Thus, a stable wavelike distribution of the SLP is established over the Northern Hemisphere. This leads to excitation of stationary wave, as a bifurcation of the flow occurs from a relatively zonal flow for the present-day to a wavelike structure under LGM conditions (Cook and Held, 1988). The westerlies from the Pacific Ocean tend to overpass the glaciers from the north, which is in agreement to other model results (e.g., Kutzbach and Wright, 1985; Manabe and Broccoli, 1985). The splitting of the flow in the luff side of the Laurentide Ice Sheet, followed by a southward displacement of a part of the flow, is weakly represented in our simulations, which is a result of the low horizontal resolution of the model. Along with the modified glacial pressure structure in the North Atlantic, the westerlies at the surface are enhanced and displaced to the south. Simulating LGM with an AGCM coupled to a mixed layer ocean, Marsiat and Valdes (1999) found stronger westerlies over the whole atmospheric column and the highest speed over the Atlantic ocean.

The flow deflection in the glacial experiments in the Northern Hemisphere is caused by the diabatic heating and/or orography and transients. The zonal asymmetries in the transient eddy vorticity fluxes play a minor role in maintaining the climatological stationary eddies (Held et al., 2002). Therefore, their contribution for the

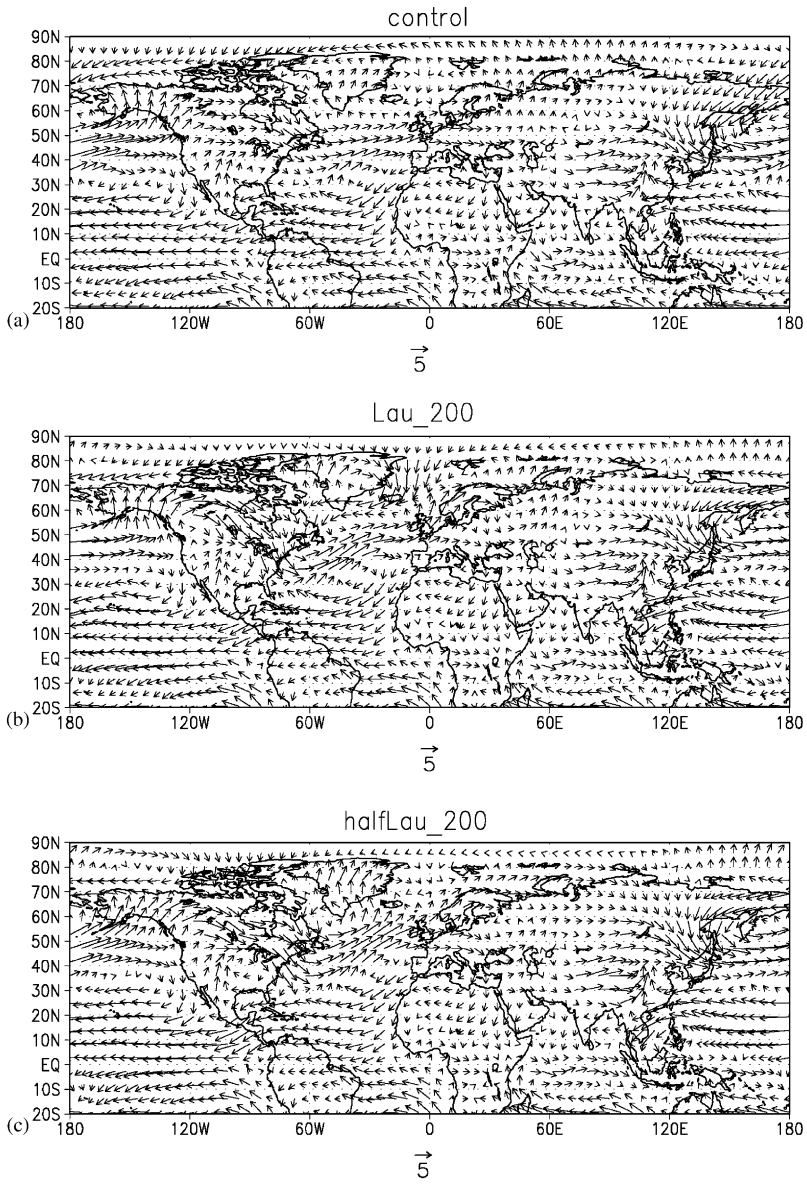

Fig. 8. Surface wind field for (a) ***control*** run; (b) ***Lau_200*** and (c) ***halfLau_200*** experiments. The fields are averaged over 25 years of integration. Units are ms^{-1}.

steady atmospheric state is not considered in this study. A separation of the thermally induced climatological changes from the orographically provoked diversion of the atmospheric flow is carried out through applying different thermal boundary conditions to the mixed layer model keeping the same orography. The analysis of the experimental results shows that the thermal heating, as given through different LGM reconstructions, could contribute from 17% to 40% for the mid-latitude and polar cooling (Table 2).

Regarding the orographic influence onto the climate, experiment ***halfLau_200***, performed with half of the height of the Laurentide Ice Sheet and the same heat flux forcing as in experiment ***Lau_200***, shows that the effect is already large enough to excite a planetary wave and an anticyclonic formation which is found over the ice sheet. The temperature over the North American continent is lowered by 80% relative to the whole cooling provoked by the 'full' height of the Laurentide Ice Sheet. Therefore, the atmospheric response to the half of the land boundary conditions is not lowered by half of the 'full' orography, which points to a non-linear behavior of the climate system relative to orographic changes.

5. Summary and conclusions

We performed AGCM simulations for present day and glacial climates using different oceanic background

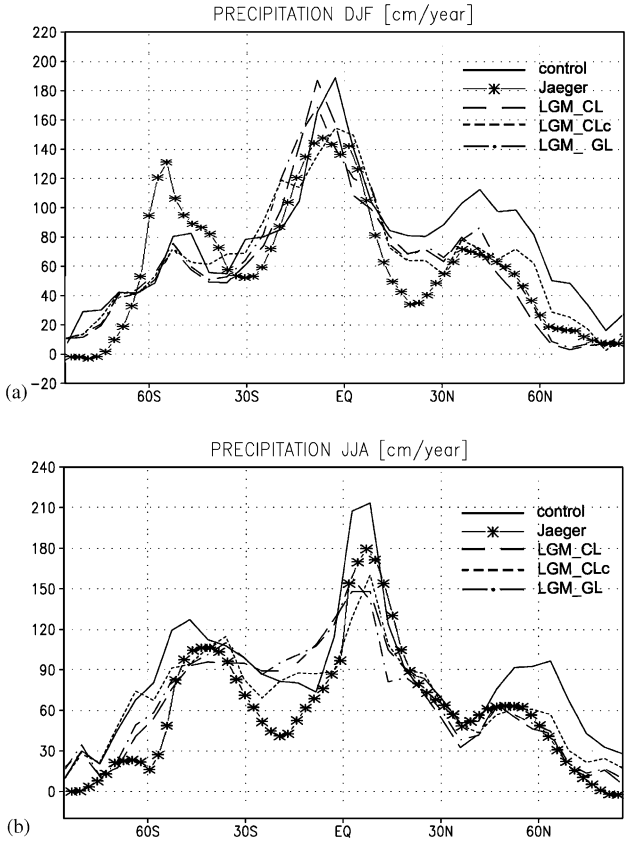

Fig. 9. Zonal mean precipitation obtained from the ***control*** run and from the experiments ***LGM_CL***, ***LGM_CLc*** and ***LGM_GL***, compared with climatological estimates of Jaeger (1976): (a) for winter and (b) summer seasons. The fields are averaged over 50 y of integration. Units are cm/year.

states and orography. The reference climate is based on present-day SSTs (Phillips et al., 1995), whereas the glacial background climate was derived from different reconstructions based on CLIMAP (1981), CLIMAP SST with additional cooling in the tropics (Lohmann and Lorenz, 2000), and the new reconstruction GLAMAP 2000 (Sarnthein et al., 1996; Paul and Schäfer-Neth, 2003). The oceanic heat transports for present-day and glacial climates are derived from OGCM simulations.

Our experiments aim to systematically analyze the role of the oceanic heat transport and orography for the glacial climate. Since coupled models show mutually inconsistent results (Hewitt et al. 2001; Kitoh et al., 2001; Shin et al., 2003), our admittedly simplified approach provides another perspective to understand the glacial climates.

We find that the elevated North American continent provokes a more wavelike Northern Hemisphere atmospheric circulation relative to a situation when the Laurentide Ice Sheet was absent. The situation is not qualitatively different from a sensitivity experiment when the height of the Laurentide Ice Sheet was reduced. In the glacial experiments, the surface flow over the North Atlantic is enhanced and displaced southward. This flow characteristics is independent of the CO_2 concentration and appears to be robust for the glacial climate.

In our first set of experiments, the oceanic heat transport is fixed to present-day conditions. Along with the wavelike Northern Hemisphere atmospheric circulation, the equatorial Pacific Ocean is warmed while the North Atlantic is cooled. Caused by a southward shift of the thermal equator during glacial times, a southward shift of the ITCZ is detected for the boreal winter season. The southward shift of the ITCZ during glacial times affects the interbasin water vapor transport which is important for the large-scale THC under glacial and present day conditions (Lohmann and Lorenz, 2000; Lohmann, 2003).

Additional to the orographic forcing, significant changes of the Northern Hemisphere circulation are induced by the glacial background climate. Assessing, separately, the relative contribution of the ocean circulation and the Laurentide Ice Sheet upon the North Atlantic climate, it is found that the changes of the orography and albedo caused even only with half height of the Laurentide Ice Sheet induce strong temperature changes of about $-16\,^{\circ}C$, whereas a reduced glacial ocean circulation with about half of present day strength induces an additional cooling of about $-4\,^{\circ}C$, only. We conclude therefore, that the strength of the oceanic thermohaline circulation is of secondary importance for the North Atlantic climate relative to the orography and albedo effects induced by the Laurentide Ice Sheet.

In our experiments we have neglected feedbacks connected with the dynamics of the ice sheet and with asynchronous development of the American, Fennoscandian, and Barents Sea Ice Sheets. However, the experiment with half of the height of the Laurentide Ice Sheet can represent a transient state of the glacial continental ice cover and the associated atmospheric reaction. Our study emphasizes the importance of reconstructing the extent and height of the continental ice sheets and including dynamical ice sheets in model experiments, rather than investigating the changes of the oceanic heat transport.

Acknowledgements

We gratefully acknowledge the suggestions and recommendations of M. Prange and F. Lunkeit. We also thank the reviewers for the suggestions and constructive comments which helped to improve the manuscript. This work has been funded through German Ministry for Education and Research (BMBF) within DEKLIM project "Climate Transitions".

References

Alley, R.B., Clark, P.U., 1999. The deglaciation of the northern hemisphere: a global perspective. Annual Reviews of Earth and Planetary Sciences 27, 149–182.

Bard, E., 1999. Ice age temperatures and geochemistry. Science 284, 1133–1134.

Barnola, J.M., Raynaud, D., Korotkevich, Y.S., Lorius, C., 1987. Vostok ice core provides 160,000 year record of atmospheric CO_2. Nature 329, 408–414.

Berger, A.L., 1978. Long term variations of daily insolation and Quaternary climatic changes. Journal of the Atmospheric Sciences 35 (12), 2362–2367.

Broccoli, A.J., 2000. Tropical cooling at the Last Glacial Maximum: an atmosphere-mixed layer ocean model simulation. Journal of Climate 13, 951–976.

Butzin, M., Prange, M., Lohmann, G., 2003. Studien zur ^{14}C-Verteilung im glazialen Ozean mit einem globalen Ozeanzirkulationsmodell. Terra Nostra 6, 86–88.

Chen, P., 2000. Thermally forced stationary waves in a quasigeostrophic system. Journal of Atmospheric Sciences 58, 1585–1594.

Chiang, J.C.H., Biasutti, M., Battisti, D.S., 2003. Sensitivity of the Atlantic ITCZ to Last Glacial Maximum boundary conditions. Paleoceanography 18.

Clark, P.U., Pisias, N.G., Stocker, T.F., Weaver, A.J., 2002. The role of the thermohaline circulation in abrupt climate change. Nature 415, 863–869.

Claussen, M., Mysak, L.A., Weaver, A.J., Crucifix, M., Fichefet, T., Loutre, M.F., Weber, S.L., Alcamo, J., Alexeev, V.A., Berger, A., Calov, R., Ganopolski, A., Goosse, H., Lohmann, G., Lunkeit, F., Mokhov, I.I., Petoukhov, V., Stone, P., Wang, Z., 2002. Earth system models of intermediate complexity: closing the gap in the spectrum of climate system models. Climate Dynamics 18, 579–586.

CLIMAP Project Members, 1981. Seasonal reconstructions of the earth's surface at the Last Glacial Maximum. Geological Society of America, Map and Chart Series, MC-36,18,18 maps.

Cook, K.H., Held, I.M., 1988. Stationary waves of the ice age climate. Journal of Climate 1, 807–819.

de Vernal, A., Hillaire-Marcel, C., 2000. Sea-ice cover, sea-surface salinity and halo/thermocline structure of the northwest North Atlantic: modern versus full glacial conditions. Quaternary Science Reviews 19, 65–68.

Eliasen, E., Machenhauer, B., Rasmussen, E., 1970. On a numerical method for integration of the hydrodynamical equations with a spectral representation of the horizontal fields. Report No. 2, Institute for Theoretical Meteorology, University of Copenhagen, 37pp.

Farrera, I., Harrison, S.P., Prentice, I.C., Ramstein, G., Guiot, J., Bartlein, P.J., Bonnefille, R., Bush, M., Cramer, W., von Grafenstein, U., Holmgren, K., Hooghiemstra, H., Hope, G., Jolly, D., Lauritzen, S.-E., Ono, Y., Pinot, S., Stute, M., Yu, G., 1999. Tropical climates at the Last Glacial Maximum: a new synthesis of terrestrial palaeoclimate data. I. Vegetation, lake-levels and geochemistry. Climate Dynamics 15, 823–856.

Fraedrich, K., Kirk, E., Lunkeit, F., 1998. Portable university model of the atmosphere. Technical Report 16, Deutsches Klimarechenzentrum, 377pp.

Franzke, C., Fraedrich, K., Lunkeit, F., 2000. Low frequency variability in a simplified atmospheric global circulation model: storm track induced 'spatial resonance'. Quaternary Journal of the Royal Meteorological Society 126, 2691–2708.

Frisius, T., Lunkeit, F., Fraedrich, K., James, I.N., 1998. Storm-track organization and variability in a simplified atmospheric global circulation model (SGCM). Quaternary Journal of the Royal Meteorological Society 124, 1019–1143.

Grosfeld, K., Lohmann, G., Romanova, V., Lunkeit, F., Fraedrich, K., 2005. Atmospheric simulations using a GCM of intermediate complexity: present day and last glacial maximum experiments, in preparation.

Held, I.M., Ting, M., 1990. Orographic and thermal forcing of stationary waves: the importance of the mean low-level wind. Journal of Atmospheric Sciences 47, 697–706.

Held, I.M., Ting, M., Wang, H., 2002. Northern winter stationary waves: theory and modeling. Journal of Climate 15, 2125–2144.

Hewitt, C.D., Broccoli, A.J., Mitchell, J.F.B., Stouffer, R.J., 2001. A coupled model study of the last glacial maximum: was part of the North Atlantic relatively warm? Geophysical Research Letters 28, 1571–1574.

Hoskins, B.J., Simmons, A.J., 1975. A multi-layer spectral model and the semi-implicit method. Quaternary Journal of the Royal Meteorological Society 101, 637–655.

Jaeger, L., 1976. Monatskarten des Niederschlags für die ganze Erde. German Weather Service Report 139, Offenbach.

Jouzel, J., Lorius, C., Petit, J.R., Genthon, C., Barkov, N.J., Kotlyakov, V.M., Petrov, V.M., 1987. Vostok ice-core: a continuous isotope temperature record over the last climatic cycle (160,000) years. Nature 329, 403–408.

Kaplan, A., Cane, M., Kushnir, Y., Clement, A., Blumenthal, M., Rajagopalan, B., 1998. Analyses of global surface temperatures 1856–1991. Journal of Geophysical Research 103, 18567–18589.

Keeling, C.D., Chin, J.F.S., Whorf, T.P., 1996. Increased activity of northern vegetation inferred from atmospheric CO_2 measurements. Nature 382, 146–149.

Kim, S.J., 2004. The effect of atmospheric CO_2 and ice sheet topography on LGM climate. Climate Dynamics (doi:10.1007/s00382-004-0412-2).

Kitoh, A., Murakami, F.S., Koide, H., 2001. A simulation of the Last Glacial Maximum with a coupled atmosphere-ocean GCM. Geophysical Research Letters 28, 2221–2224.

Knorr, G., Lohmann, G., 2003. Southern Ocean origin for resumption of Atlantic thermohaline circulation during deglaciation. Nature 424, 532–536.

Knorr, G., Grosfeld, K., Lohmann, G., Lunkeit, G., Fraedrich, K., 2005. Atmospheric response to abrupt changes in the thermohaline circulation during deglaciation. Geochemistry, Geophysics, Geosystems, in revision.

Kutzbach, J.E., Wright, H.E., 1985. Simulation of the climate of 18,000 BP: results from the North American/North Atlantic/European sector and comparison with the geologic record. Quaternary Science Reviews 4, 147–187.

Leonard, B.P., 1979. A stable and accurate convective modelling procedure based on quadratic upstream interpolation. Computer Methods in Applied Mechanics and Engineering 19, 59–98.

Lohmann, G., 2003. Atmospheric and oceanic freshwater transport during weak Atlantic overturning circulation. Tellus 55A, 438–449.

Lohmann, G., Lorenz, S., 2000. On the hydrological cycle under paleoclimatic conditions as derived from AGCM simulations. Journal of Geophysical Research 105, 417–436.

Lorenz, S., Lohmann, G., 2004. Reconciling glacial snow lines with tropical sea surface temperatures. Geochemistry, Geophysics, Geosystems, revised.

Lunkeit, F., Bauer, S.E., Fraedrich, K., 1998. Storm tracks in a warmer climate: sensitivity studies with a simplified global circulation model. Climate Dynamics 14, 813–826.

Maier-Reimer, E., Mikolajewicz, U., Hasselmann, K., 1993. Mean circulation of the Hamburg LSG OGCM and its sensitivity to the thermohaline surface forcing. Journal of Physical Oceanography 23, 731–757.

Manabe, S., Broccoli, A.J., 1985. The influence of continental ice sheets on the climate of an ice age. Journal of Geophysical Research 90, 2167–2190.

Marsiat, I., Valdes, P.J., 1999. Sensitivity of the Northern Hemisphere climate of the Last Glacial Maximum to sea surface temperatures. Climate Dynamics 17, 233–248.

Mix, A.C., Morey, A.E., Pisias, N.G., Hostetler, S.W., 1999. Foraminiferal faunal estimates of paleotemperature: circumventing the no-analog problem yields cool ice age tropics. Paleoceanography 14, 350–359.

Mix, A.C., Bard, E., Schneider, R., 2001. Environmental processes of the ice age: land, oceans, glaciers (EPILOG). Quaternary Science Reviews 20, 627–657.

Nigam, S., Held, I.M., Lyons, S.W., 1987. Linear simulation of the stationary eddies in a GCM. Part I: The "no-mountain" model. Journal of Atmospheric Science 43, 2944–2961.

Orszag, S.A., 1970. Transform method for calculation of vector-coupled sums: application to the spectral form of the vorticity equation. Journal of Atmospheric Sciences 27, 890–895.

Paul, A., Schäfer-Neth, C., 2003. Modeling the water masses of the Atlantic Ocean at the Last Glacial Maximum. Paleoceanography 18 (3), 1058.

Peltier, W.R., 1994. Ice age paleotopography. Science 265, 195–201.

Pflaumann, U., Sarnthein, M., Chapman, M., d'Abreu, L., Funnell, B., Huels, M., Kiefer, T., Maslin, M., Schulz, H., Swallow, J., van Kreveld, S., Vautravers, M., Vogelsang, E., Weinelt, M., 2003. Glacial North Atlantic: sea-surface conditions reconstructed by GLAMAP 2000. Paleoceanography 18 (3), 1065.

Phillips, T.J., Anderson, R., Brösius, M., 1995. Hypertext summary documentation of the AMIP models. UCRL-MI-116384, Lawrence Livermore National Laboratory, Livermore, CA.

Prange, M., Romanova, V., Lohmann, G., 2002. The glacial thermohaline circulation: stable or unstable? Geophysical Research Letters 29 (21), 2028.

Prange, M., Lohmann, G., Paul, A., 2003. Influence of vertical mixing on the thermohaline hysteresis: analyses of an OGCM. Journal of Physical Oceanography 33 (8), 1707–1721.

Prange, M., Lohmann, G., Romanova, V., Butzin, M., 2004. Modelling tempo-spatial signatures of Heinrich events: influence of the climatic background state. Quaternary Science Reviews 23/5–6, 521–527.

Roeckner, E., Arpe, K., Bengtsson, L., Brinkop, S., Dümenil, L., Esch, M., Kirk, E., Lunkeit, F., Ponater, M., Rockel, B., Sausen, R., Schlese, U., Schubert, S., Windelband, M., 1992. Simulation of present-day climate with the ECHAM model: impact of model physics and resolution. MPI Report No. 93, ISSN 0937-1060, Max-Planck-Institut für Meteorologie, Hamburg, Germany, 171pp.

Romanova, V., Prange, M., Lohmann, G., 2004. Stability of the glacial thermohaline circulation and its dependence on the background hydrological cycle. Climate Dynamics 22, 527–538.

Sarnthein, M., Gersonde, R., Niebler, S., Pflaumann, U., Spielhagen, R., Thiede, J., Wefer, G., Weinelt, M., 2003. Overview of Glacial Atlantic Mapping (GLAMAP 2000). Paleoceanography 18, 1030.

Schäfer-Neth, C., Paul, A., 2001. Circulation of the glacial Atlantic: a synthesis of global and regional modeling. In: Schaefer, P., Ritzrau, W., Schlueter, M., Thiede, J. (Eds.), The Northern North Atlantic: A Changing Environment. Springer, Berlin, pp. 446–462.

Shin, S., Liu, Z., Otto-Bliesner, B.L., Brady, E.C., Kutzbach, J.E., Harrison, S.P., 2003. A simulation of the Last Glacial Maximum climate using the NCAR-CCSM. Climate Dynamics 20, 127–151.

Valdes, P.J., Hoskins, B.J., 1989. Linear stationary wave simulations of the time-mean climatological flow. Journal of Atmospheric Science 46, 2509–2527.

Weinelt, M., Sarnthein, M., Pfaumann, U., Schulz, H., Jung, S., Erlenkeuser, H., 1996. Ice-free Nordic Seas during the Last Glacial Maximum? Potential sites of deepwater formation. Palaeoclimates 1, 283–300.